A&A 406, 1019–1031 (2003)
DOI: 10.1051/0004-6361:20030742

Astronomy & Astrophysics

Discovery of a magnetic field in the Slowly Pulsating B star ζ Cassiopeiae*

C. Neiner[1,2,3], V. C. Geers[1], H. F. Henrichs[1], M. Floquet[2], Y. Frémat[2], A.-M. Hubert[2], O. Preuss[4], and K. Wiersema[1]

[1] Sterrenkundig Instituut "Anton Pannekoek", Universiteit van Amsterdam, The Netherlands
[2] GEPI/ UMR 8111 du CNRS, Observatoire de Paris-Meudon, 92195 Meudon Cedex, France
[3] Current affiliation: RSSD, Estec/ESA, Keplerlaan 1, 2201 AZ, Noordwijk ZH, The Netherlands
[4] Max Plank Institut für Aeronomie, Lindau, Germany

Received 13 August 2002 / Accepted 16 May 2003

Abstract. ζ Cas is a B2 IV star with $v \sin i = 17$ km s^{-1}. Time-resolved circular spectropolarimetric observations of ζ Cas obtained in 2001 and 2002 with the Musicos échelle spectropolarimeter at the 2 m Télescope Bernard Lyot (TBL) show a sinusoidally varying longitudinal magnetic field with a strength between 10 G and −46 G for the averaged line-of-sight component, corresponding to $B_{\rm pol} = 335^{+120}_{-65}$ G. The period corresponds very accurately with the 5.37045 day period as derived from stellar wind variations observed in the ultraviolet. The epoch of the positive maximum field corresponds in phase with the maximum emission in the UV wind lines. This gives compelling evidence for a magnetic rotator model for this star, with an unambiguous rotation period of 5.37 days. We searched for periodicity in line-profile variations (lpv), radial velocity and minimum intensity curves in the ∼400 optical spectra. We found a non-radial pulsation mode with $l = 2 \pm 1$ at the frequency $f = 0.64$ c d^{-1}. From this periodicity and from stellar parameters derived from model fits, we propose to classify ζ Cas as a Slowly Pulsating B (SPB) star. This is the third detection of a magnetic field in an early B-type pulsating star and the first one in a SPB star.

Key words. stars: magnetic fields – stars: oscillations – stars: winds, outflows

1. Introduction

The B2 IV-V star ζ Cas (HD 3360) has been classified as a 53 Per variable by Smith & Karp (1976). This type of O8 to B5 variables show variability in line profiles with variable periods of the order of a day, associated with non-radial pulsations. The line profile of the Si III 4553 line of ζ Cas was found to be variable by Smith & Karp (1976) with a period of 21.5 hours (Smith 1980). Sadsaoud et al. (1994) investigated the light and line-profile variability in 1990 and 1991. The light fluctuations were found to be less than 0.004 mag and no period could be detected. The full width at half maximum of the Si III 4553 line was found variable from night to night and also during each single night. To reproduce such variations a 0.27 day period was proposed, possibly due to a non-radial pulsation g mode, in addition to an orbital motion. The authors argued that the shape of the Si III 4553 line profile variations confirms the 53 Per variable type. Note that most of the 53 Per variables were later included in the class of SPB stars by Waelkens (1991).

The C IV UV resonance doublet was reported to be variable by Grady et al. (1987) and Sonneborn et al. (1987), who set an upper limit of several months on the variability. Its spectral type was determined independently by Rountree & Sonneborn (1991) from UV spectra as B2 IVw where w indicates an abnormally strong Si IV and N V absorption for its type. Gies & Lambert (1992) found that ζ Cas is N-enriched and O-weak, whereas Andrievsky et al. (1999) found that it is C-weak.

The specific wind behavior and the chemical enrichment in some elements are two indirect indicators of the presence of a magnetic field in this type of star (Henrichs 2001). These considerations motivated us to undertake a detailed time-resolved UV study of ζ Cas, which was regularly monitored with the IUE satellite as a standard star, and to attempt to measure its magnetic field with the Musicos spectropolarimeter at TBL (Pic du Midi, France).

In addition, studying the pulsation properties of a rotating magnetic star gives strong constraints on its stellar parameters and its evolutionary stage, which is of high asteroseismological importance. Therefore we also analysed the pulsation properties of the star.

We present the UV and spectropolarimetric observations in Sect. 2. We analyse the stellar wind changes and extract the rotational period in Sect. 3. We review the stellar parameters in Sect. 4 and present our attempt to determine a consistent set

Send offprint requests to: C. Neiner,
e-mail: cneiner@rssd.esa.int

* Based on observations obtained using the Musicos spectropolarimeter at the Observatoire du Pic du Midi, France, and on INES data from the International Ultraviolet Explorer (IUE) satellite.

of parameters. We also analyse the chemical composition. In Sect. 5 we study the stellar pulsations in the line-profile variability, radial velocity and minimum intensity measurements. In Sect. 6 we report on the measurements of the longitudinal component of the discovered magnetic field, in the context of an oblique magnetic dipole. In Sect. 7, we discuss our results and draw conclusions.

2. Observations

2.1. Ultraviolet spectroscopy

High-dispersion ultraviolet spectra ($R \simeq 18\,000$) were obtained with the Short Wavelength Prime (SWP) camera onboard the IUE satellite. Table 2 presents the journal of 103 spectra of ζ Cas obtained from 1979 to 1995. 22 other available spectra were discarded because of lower quality (under- or overexposed). The exposure time was 23.6 s, except for SWP 1722 and 1724 which were exposed 29.8 s, SWP 5468 and 17867 which were exposed 20.8 s and SWP 40854 which was exposed 24.9 s. All reduced data were retrieved from the INES database. The spectra were mapped on an uniform wavelength grid of 0.1 Å, which effectively degraded the resolving power to 12 000−15 000. The signal-to-noise ratio of the spectra in well exposed regions is about 15.

2.2. Spectropolarimetry

The fiber-fed Musicos échelle spectropolarimeter ($R = 35\,000$) is mounted at the Cassegrain focus of the 2 m Télescope Bernard Lyot (TBL) at the Pic du Midi in France (see Donati et al. 1999). Stellar light is collected in a 2″ entrance aperture in the spectral range 4500−6600 Å. Linear/circular sheet polarisers can be inserted in the beam. One half-wave and one quarter-wave retarder can also be inserted and rotated to achieve a linear or circular analysis of the stellar light.

To detect stellar magnetic fields, one analyses the circular polarisation of the light. The light is split into two beams, fed to the spectrograph through a double optical fiber and simultaneously recorded onto the 1024 × 1024 24 μm square pixel SITe CCD detector. The observing strategy is to set the quarter-wave plate and take 4 exposures: one at azimuth -45°, two at azimuth 45°, and one more at azimuth -45°. In principle only 2 exposures are needed (one at each azimuth) but with 4 exposures the path of the two beams are mutually exchanged through the instrument during one complete Stokes V measurement. With this procedure, systematic spurious circular polarisation signals are removed down to an accuracy of 0.002%.

27 Stokes V measurements were obtained in June–July 2001 (observers CN, HH, VG), 17 Stokes V measurements were obtained in December 2001 (observer CN), and 74 measurements were obtained in June 2002 (observers VG, KW, HH), i.e. 118 in total (see top part of Table 1). The exposure time was 300 s, except for the measurements 15, 24, 27, 48, 53 and 57 for which it was 240 s, and for the measurements 81 to 84, 86 to 104, 106 to 110 and 112 to 118 for which it was 420 s. The average signal-to-noise ratio of a complete measurement is in the range 350−400 in the intensity continuum, for an exposure time of about 300 s.

Table 1. Journal of TBL observations of ζ Cas obtained in 2001 and 2002. Top table: complete Stokes V sets used for magnetic analysis. Bottom table: additional individual spectra used for pulsation analysis. When several sets/spectra were obtained the same night, only the mid-HJD of the first one is given, the other ones being taken consecutively. The mid-HJD is given minus 2 452 000 d.

Sets #	Mid HJD	Sets #	Mid HJD	Sets #	Mid HJD
1−2	82.59	32−33	253.34	62−66	440.59
3−5	85.61	34−35	255.38	67−71	441.59
6−9	86.59	36−37	257.42	72−76	442.58
10	87.63	38−39	261.38	77−80	443.60
11−12	88.64	40	264.28	81−84	444.57
13−14	89.62	41−42	265.25	85	444.66
15	89.65	43−44	266.26	86−89	446.56
16−18	90.62	45−47	436.59	90−94	447.56
19−21	91.61	48	436.64	95−99	448.56
22−23	92.62	49−52	437.59	100−104	450.55
24	92.66	53	437.66	105	450.66
25−26	93.62	54−55	438.60	106−110	451.56
27	93.65	56	438.64	111	451.66
28−29	249.39	57	438.66	112−114	452.61
30−31	251.38	58−61	439.61	115−118	453.56
Mid-HJD		87.62	88.58	438.62	440.57
Numb. spectra		4	1	3	2

The individual subexposures can also be used as normal spectroscopic data, including subexposures which do not form a complete set for a magnetic measurement. The latter ones are listed in the bottom part of Table 1. Therefore we have 113 individual spectra in June–July 2001 and 302 in 2002, i.e. 415 in total which can be used for pulsation analysis. The number of spectra obtained in December 2001 is too small to be usefully included for this purpose.

After applying a cross-correlation technique, such as the Least-Squares Deconvolution (LSD) developed by Donati et al. (1997), one can detect stellar magnetic fields through the Zeeman signatures generated in the shape and polarisation state of spectral line profiles (see Fig. 10). A dedicated software package, ESpRIt, is available at TBL to reduce and analyse the data. We used an improved version of ESpRIt, which optimized the extraction by using two sets of flat-fields taken in the two polarimeter positions. We also corrected for the fringes by creating a fringe template from the spectrum of a non-magnetic star (Vega) reduced in the same way as the target star. For the data obtained in 2001, one fringe template was obtained and used for the whole run, while in 2002 Vega was observed every night and the fringe template was adjusted each night.

Table 2. Journal of IUE observations of ζ Cas used in this paper and equivalent widths measurements. Column 1 indicates the number of the spectrum in the IUE archives. The Heliocentric Julian Date (HJD) at mid-exposure minus 2 440 000 is given in Col. 2, whereas Col. 3 indicates the rotational phase. Columns 4 and 5 give the equivalent width in Å and its error bar.

Image SWP	Mid HJD	Rot. phase	EW (Å)	σEW (Å)	Image SWP	Mid HJD	Rot. phase	EW (Å)	σEW (Å)	Image SWP	Mid HJD	Rot. phase	EW (Å)	σEW (Å)
1722	3664.82	0.830	1.86	0.30	27544	6448.78	0.216	2.09	0.29	40854	8298.53	0.647	2.55	0.28
1724	3664.92	0.850	1.67	0.31	27697	6472.58	0.647	2.52	0.28	42002	8442.98	0.545	2.27	0.28
5468	4034.67	0.697	2.46	0.27	28627	6619.01	0.913	1.29	0.33	42175	8474.07	0.332	2.27	0.29
7807	4268.40	0.219	1.82	0.30	28830	6647.18	0.159	1.95	0.30	42485	8517.02	0.331	2.58	0.27
8964	4369.53	0.050	1.19	0.34	29264	6694.22	0.917	1.53	0.32	42780	8551.82	0.809	2.02	0.29
13317	4651.63	0.578	2.31	0.28	29275	6695.15	0.091	1.57	0.32	43161	8580.93	0.230	2.45	0.27
13928	4733.24	0.774	2.45	0.27	30118	6814.73	0.356	2.45	0.28	43294	8592.86	0.453	2.53	0.27
14277	4774.49	0.456	2.47	0.28	30330	6844.53	0.906	1.74	0.31	43542	8624.53	0.349	2.25	0.28
15874	4963.23	0.599	2.39	0.28	31525	7017.11	0.040	1.33	0.33	44006	8669.43	0.710	2.71	0.28
16298	5010.23	0.351	2.36	0.28	32178	7096.90	0.897	1.50	0.32	45055	8806.21	0.179	1.92	0.30
16299	5010.41	0.384	2.35	0.28	32365	7119.89	0.180	1.97	0.30	45271	8838.07	0.111	1.41	0.33
17074	5120.47	0.878	1.62	0.31	33883	7351.98	0.396	2.29	0.28	45538	8871.98	0.425	2.40	0.28
17867	5220.13	0.436	2.53	0.27	33973	7370.17	0.782	2.31	0.28	46052	8920.51	0.462	2.44	0.28
18654	5298.78	0.080	1.45	0.32	34025	7379.09	0.442	2.42	0.28	46263	8940.55	0.194	1.98	0.30
19316	5389.46	0.966	1.62	0.31	34026	7379.13	0.451	2.42	0.28	46564	8979.82	0.505	2.21	0.29
20079	5481.45	0.094	1.40	0.33	34027	7379.18	0.459	2.39	0.28	46660	8992.70	0.904	1.78	0.31
20715	5565.94	0.827	1.89	0.30	34151	7403.67	0.019	1.61	0.32	46868	9020.47	0.074	1.40	0.33
20993	5587.36	0.815	1.95	0.30	34272	7423.91	0.788	2.32	0.28	48037	9173.23	0.519	2.15	0.29
21214	5609.88	0.008	1.12	0.34	34749	7481.93	0.592	2.32	0.28	48278	9200.95	0.682	2.45	0.28
21627	5665.79	0.419	2.15	0.29	36807	7745.84	0.733	2.40	0.28	48583	9239.07	0.779	2.16	0.29
21631	5665.86	0.433	2.12	0.29	36818	7748.90	0.304	2.57	0.28	48980	9282.99	0.957	1.65	0.31
21867	5693.64	0.605	2.31	0.28	37215	7799.96	0.811	1.96	0.30	49685	9346.81	0.842	1.82	0.30
22047	5718.79	0.287	2.13	0.29	37279	7807.98	0.305	2.41	0.28	49953	9387.57	0.431	2.51	0.28
22249	5742.50	0.704	2.47	0.28	37532	7837.72	0.842	2.00	0.29	51309	9538.01	0.442	2.37	0.28
23145	5853.25	0.324	2.41	0.28	37716	7862.66	0.485	2.40	0.28	51658	9564.07	0.295	2.28	0.29
23376	5883.06	0.875	1.63	0.31	38143	7928.33	0.715	2.36	0.28	51760	9573.96	0.137	2.05	0.29
24251	5994.94	0.709	2.57	0.27	39189	8079.65	0.890	1.60	0.32	52372	9636.76	0.831	1.92	0.30
24915	6082.61	0.033	1.40	0.33	39214	8083.21	0.553	2.33	0.28	53015	9695.58	0.784	2.33	0.29
26331	6248.22	0.869	1.42	0.33	39394	8108.07	0.182	2.12	0.29	53257	9720.41	0.407	2.25	0.29
26510	6278.15	0.444	2.61	0.27	39620	8147.10	0.449	2.27	0.28	53298	9725.62	0.376	2.20	0.29
26905	6348.02	0.453	2.19	0.29	39863	8183.80	0.284	2.41	0.28	53874	9758.40	0.481	2.43	0.28
27045	6376.87	0.826	2.14	0.29	40087	8204.89	0.210	2.30	0.28	55665	9952.89	0.696	2.78	0.27
27198	6400.98	0.315	2.59	0.27	40435	8247.81	0.202	2.09	0.29	56219	10043.48	0.563	2.69	0.27
27379	6424.77	0.744	2.35	0.28	40656	8278.77	0.968	1.41	0.33	56343	10077.15	0.833	2.08	0.29
27543	6448.75	0.211	2.05	0.29										

The LSD method combines the very small circularly polarised signatures, properly weighted, of all available line profiles in the spectrum to increase the signal to noise ratio. For ζ Cas, we identified 281 different spectral lines and used 342 line profiles, with a number of double occurrences in subsequent échelle orders, for the construction of a mean Stokes V profile. These photospheric lines correspond to ions of He I, C II, C III, N II, O II, Ne I, Mg II, Al III, Si II, Si III, S II, Ar II, Fe III, with line depths from 0.01 to 0.46 and Landé factors from 0.5 to 2.7. The line depths and Landé factors are extracted from Kurucz models provided in the ESpRIT Package. The method assumes that the intrinsic broadening is similar for all lines. When a magnetic field is present, the Stokes V profile indicates a Zeeman signature (see Fig. 10).

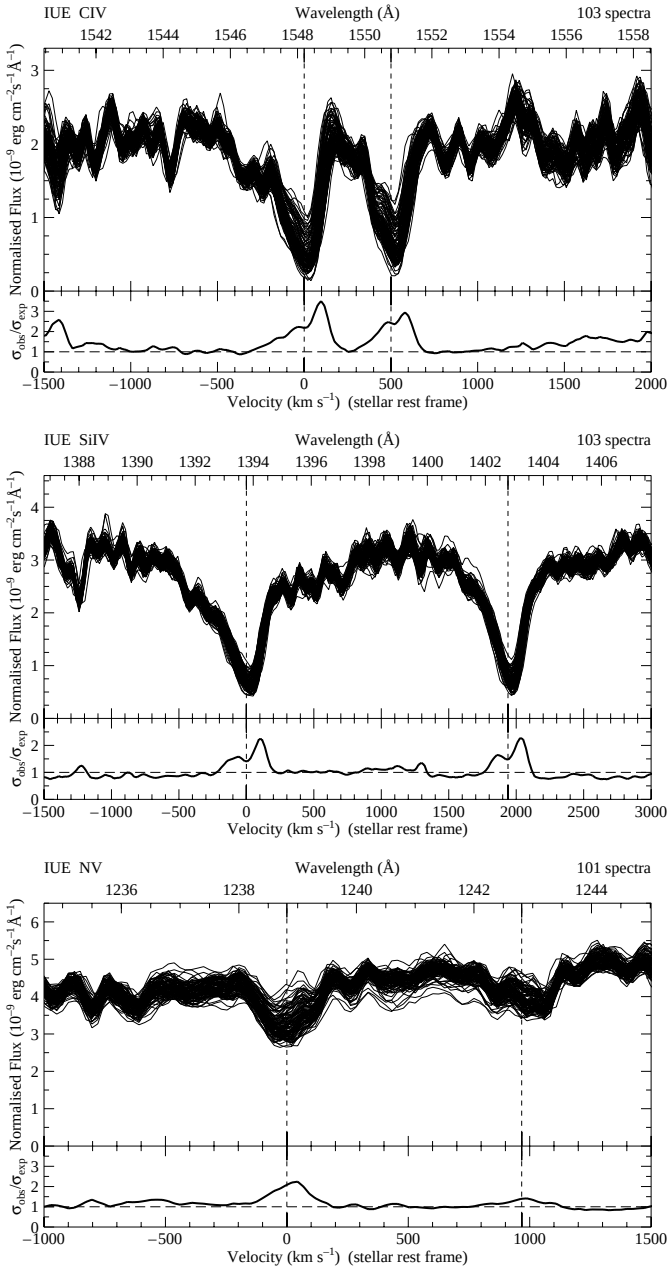

Fig. 1. Top panels: variation in the wind profiles of the UV C IV, Si IV and N V lines; the fluxes are normalised to the mean of all used spectra. Bottom panels: ratio of observed to expected variance as a measure of variability.

3. UV stellar wind

3.1. Wind variations

The variability in the UV resonance lines of ζ Cas was noticed by Grady et al. (1987) and Sonneborn et al. (1987). Out of 125 available archival IUE images we selected 103 spectra with approximately the same exposure level to obtain a homogeneous set suitable for further analysis.

Investigation of the wavelength range from 1150 Å to 1900 Å by considering the ratio of the measured to the expected variance revealed that only the regions around the C IV 1550, Si IV 1400 and N V 1240 doublets show a statistically significant signature of variability. We used a noise model for high-resolution IUE spectra as described by Henrichs et al. (1994) with parameters $A = 19$, representing the maximum averaged signal to noise, and $B = 1.6 \times 10^{-9}$, representing the average flux level. The regions around the wind sensitive Si III 1206 line and the C III 1175 complex are too heavily saturated and background contaminated to allow a reliable study. The Al III 1860 doublet was not found to be variable. The top panels of Fig. 1 show an overplot of the C IV, Si IV and N V profiles, respectively, along with the variability signatures in the bottom panels. The variability occurs mainly in the strength of the line over a given range in velocity space, extending from −500 to +700 km s^{-1} for C IV, and from −200 to +200 km s^{-1} around the two members of the other two doublets.

We measured the equivalent width (*EW*) in Å over these intervals, at flux level 2 for C IV, flux level 2 for Si IV, and 4 for N V lines, all in units of 10^{-9} erg cm^{-2} s^{-1} Å^{-1}. We applied the method described by Chalabaev & Maillard (1983) to calculate the error bars. The results for C IV, used for the final analysis, are included in Table 2. Although at first sight the profile changes appear to be rather small, the *EW* changes are very significant (see Fig. 2).

3.2. Rotational period

We searched for periodicity in the measured *EW* of the C IV, Si IV and N V lines. A CLEAN analysis indicated a very strong period around 5.37 days, which was used as a starting value to refine the period determination. A single sinusoid would not fit the data. Therefore we used the following function:

$$f(t) = a + b\sin\left(2\pi\left(\frac{t}{P} + \phi_1\right)\right) + c\sin\left(2\pi\left(\frac{t}{P/2} + \phi_2\right)\right). \qquad (1)$$

We used a least-square method which uses weights according to the error bars assigned to each datapoint. With given initial starting values for the free parameters a steepest descent technique searches for the lowest minimum of the χ^2. The variance matrix provides the formal errors in the free parameters.

The results of the best solution for the C IV doublet, with a reduced $\chi^2 = 0.27$, are: $a = 2.080 \pm 0.016$ Å, $b = 0.518 \pm 0.023$ Å, $\phi_1 = 0.162 \pm 0.021$, $c = 0.246 \pm 0.023$ Å, and $\phi_2 = 0.615 \pm 0.042$ with a period $P = 5.370447 \pm 0.000078$ d, where we used values of t relative to the first observation. The very high precision of the period estimate (error less than 7 s) is due to the fact that the star was observed during 17 years with the IUE satellite as a standard calibration star, which extends the coverage over 1194 cycles. A period analysis of the other two lines showed the same periods, but with lower accuracy due to the weaker signal. We therefore adopt the value obtained from the C IV analysis as the best period, which is identified with the rotation period of the star. The *EW* values as a function of rotational phase are given in Table 2 and plotted in Fig. 2. Like in the similar stars β Cep (Henrichs et al. 2000) and V 2052 Oph (Neiner et al. 2003), the *EW* of these lines folded in phase with the rotation period shows two unequal

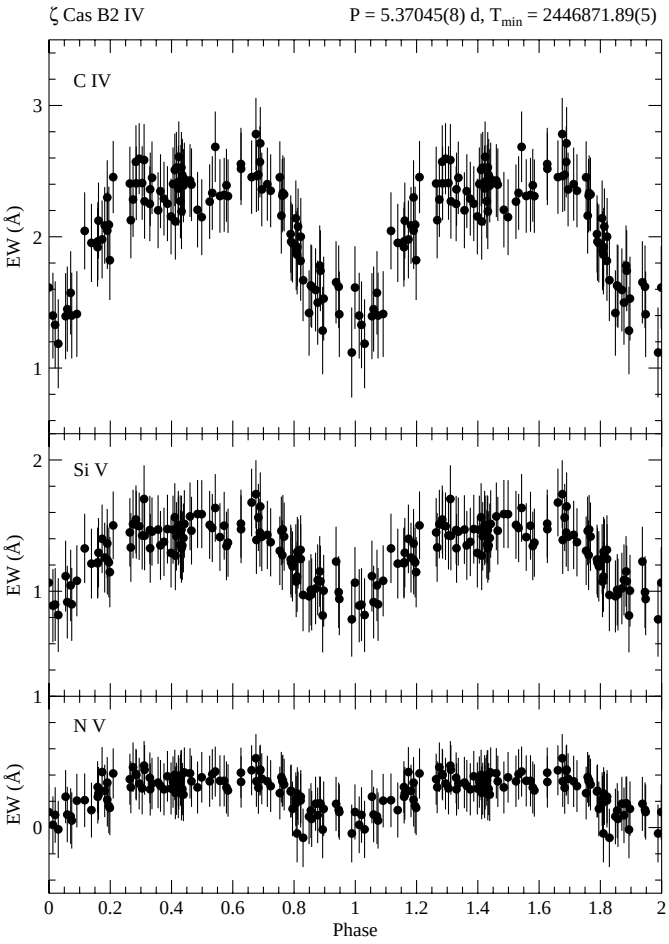

Fig. 2. Equivalent width variations of the UV C IV, Si IV and N V lines, folded in phase with the rotation period.

minima and maxima. This is typical for magnetic rotators (see below). The position of the deepest minimum (i.e. minimum absorption) in the C IV *EW* is the best defined and is used as the reference point in rotational phase.

With the analytic description given above the epoch of minimum in *EW* could be derived mathematically, which we define as the zero phase of the rotation. The derived ephemeris for calculating the rotational phase used in this paper is:

$$T(EW_{\rm min}) = \mathrm{HJD}\ 2\,446\,871.889 \pm 0.054 + N \times 5.370447 \pm 0.000078, \quad (2)$$

where N is an integer.

4. Stellar parameters

The star ζ Cas is a B2 IV-V star with $V = 3.63$ (see Table 3). Its stellar parameters have been determined in several studies, most recently by Merezhin (2000). Fitzpatrick & Massa (1999) derived $T_{\rm eff} = 20\,900 \pm 180$ and $\log g = 3.44 \pm 0.09$ by fitting Kurucz models to UV and optical spectral data. The radial velocity of the star is 2 km s^{-1} (Duflot et al. 1995).

The effective temperature, gravity and luminosity of this star place it just between the instability strips of β Cep and SPB stars (Pamyatnykh 1999). However, the fact that a possible non-radial pulsation mode has been detected, and that the star may have different periods, all of the order of a day (typical for SPB stars) suggests that it is a SPB star, rather than a β Cep star, which is characterised by a radial mode with a period of a few hours.

Table 3. Stellar parameters of ζ Cas (HD 3360, HR 153).

	This study	Literature	
Spectral Type		B2IV	G
V		3.59-3.68	BSC
Distance (pc)		183^{+206}_{-165}	Hip
$T_{\rm eff}$ (K)	20426 ± 850	21480 ± 345	M
$\log g$	3.81 ± 0.11	3.75 ± 0.07	M
$\log L/L_\odot$	3.74 ± 0.16	3.92	
$R/R_\odot$	5.9 ± 0.7	6.1 ± 0.3	M
$M/M_\odot$	8.3 ± 0.6	9.1 ± 0.1	M
$v\sin i$ (km s^{-1})	17 ± 3	16	M
$P_{\rm rot}$ (d)	5.37045		
	±0.00008		
i (°)	18 ± 4	4	M
v (km s^{-1})	55 ± 28		

G: Garcia (1989), BSC: Hoffleit & Jaschek (1991),
Hip: Perryman & ESA (1997), M: Merezhin (2000).

We determine the effective temperature of ζ Cas by fitting the slope of the TD1 UV spectrum with theoretical fluxes computed by Kurucz (1994). TD1 observations are corrected for interstellar reddening assuming a colour excess $E(B-V) = 0.03$ derived from the calibrations of Papaj et al. (1990) and using extinction laws given by Cardelli et al. (1989) and by O'Donnell (1994). Once the effective temperature is known, the gravity is estimated by combining the computed angular diameter of ζ Cas with its trigonometric parallax measured with the HIPPARCOS satellite, which give the radius, and the evolutionary tracks from Schaller et al. (1992), which give the mass. The knowledge of the radius, associated to the rotational period derived in the previous section, provides a determination of the inclination angle i. Our results are summarized in Table 3 and compared to the values used by other authors.

We then compute a NLTE model atmosphere and NLTE spectra with the TLUSTY198 and SYNSPEC45 (Hubeny & Lanz 1995) computer codes. Except for neutral oxygen which is treated with the MODION IDL package, the atomic models we use are those proposed by Hubeny & Lanz on TLUSTY's web site: H: 16 levels, He I: 24 levels, He II: 20 levels, C I: 8 levels, C II: 34 levels + 5 superlevels, C III: 12 levels, N I: 13 levels, N II: 35 levels + 14 superlevels, N III: 11 levels, O I: 14 levels + 8 superlevels, O II: 36 levels + 14 superlevels, O III: 9 levels, Si I: 6 levels, Si II: 36 levels + 4 superlevels, Si III: 12 levels.

We use an averaged spectrum of the data obtained in 2002. Helium lines are first fitted in order to derive the He/H ratio

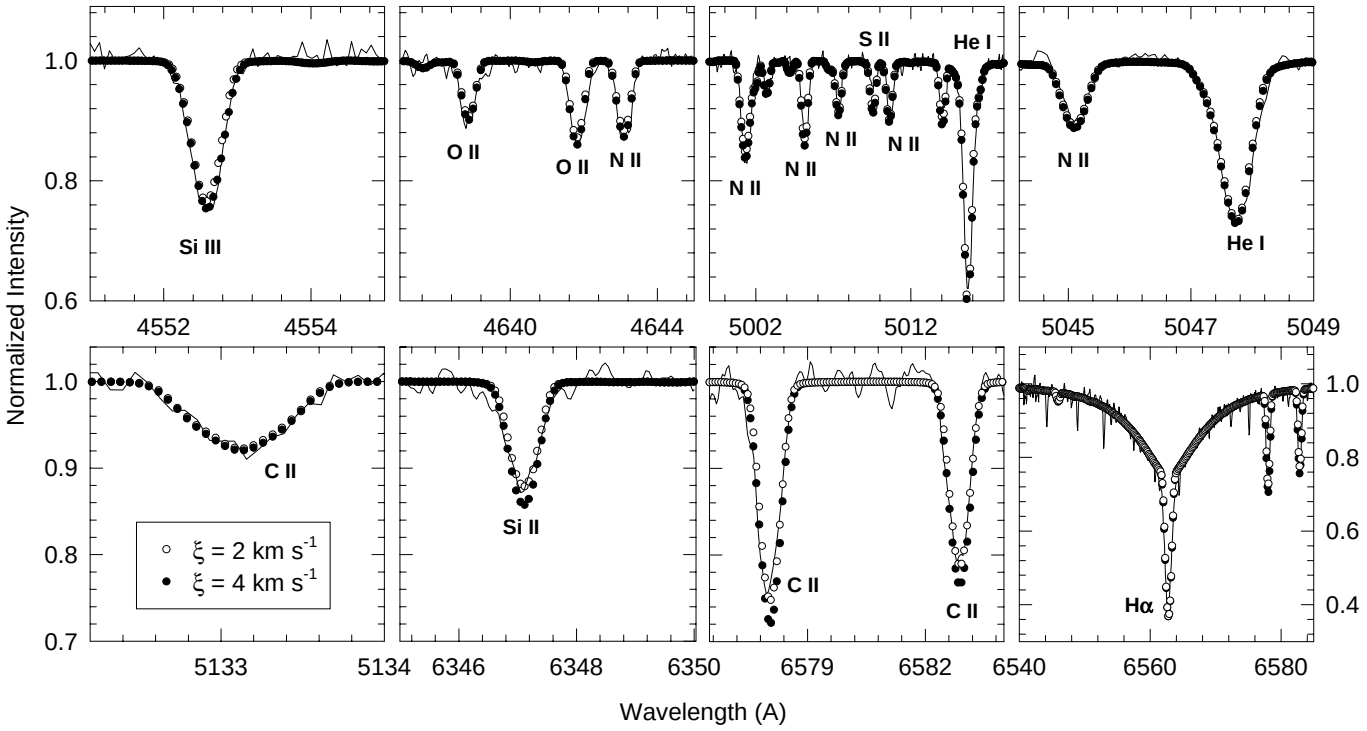

Fig. 3. Fitted spectral regions. TBL observations (solid line) are compared to the resulting theoretical spectra (dots). We adopted $\xi = 2$ km s^{-1} as the best value for the microturbulence velocity.

Table 4. Chemical composition of ζ Cas. Column 2 gives the number N of lines used to determine the abundance. The logarithmic abundances are given relatively to the solar values compiled by Grevesse & Sauval (1998).

		$\log(\epsilon_N/\epsilon_\odot)$		
Ion	N	This study	GL92	K99 & A99
He I	4	0.11 ± 0.06	-0.01 ± 0.13	
C II	3	-0.05 ± 0.09	-0.09 ± 0.10	-0.33 ± 0.08
N II	6	0.41 ± 0.10	0.34 ± 0.06	0.06 ± 0.11
O II	5	-0.09 ± 0.14	$-0.34 \pm 0.09^*$	-0.43 ± 0.09

*: LTE value, GL92: Gies & Lambert (1992),
K99: Korotin et al. (1999) for O,
A99: Andrievsky et al. (1999) for C and N.

and the projected rotation velocity (see Table 3). The Si II 6347 and Si III 4553 lines are computed with a solar chemical composition (Grevesse & Sauval 1998) and compared to the observations in order to test the validity of the adopted fundamental parameters (Fig. 3). C, N and O abundances are deduced by fitting the line profiles of several transitions (Fig. 3). The oscillator strengths used are from the NIST database and were added to the updated Kurucz line lists provided with SYNSPEC. Stark widths of the Si II and Si III spectral lines are derived from the results of González et al. (2000), Dimitrijevic et al. (2003) and Lanz et al. (1988).

We adopt a 2 km s^{-1} microturbulence velocity, in fair agreement with the value 2.7 ± 0.5 km s^{-1} given by Fitzpatrick & Massa (1999), which allows us to fit simultaneously the different studied transitions. The C II 6578 and 6583 lines appear to be the most sensitive to microturbulence. The abundances we derive are given in Table 4 and compared to previous results from the literature. ζ Cas is significantly nitrogen overabundant, even when adopting other sets of fundamental parameters, as already found by Gies & Lambert (1992). The differences between our determination and the previous ones concerning carbon and oxygen are mainly due to a different choice of the microturbulence velocity (Korotin et al. 1999) or to different effective temperature and gravity determinations (Gies & Lambert 1992). Contrary to these studies, we find that the oxygen and carbon have solar abundances, but that ζ Cas is slightly He enriched.

5. Spectral variations

5.1. Line profiles

The individual spectra from TBL were used to search for periodicity in the line profile variations of the star with two methods: the Restricted Local Cleanest (RLC, based on Foster 1995, 1996, developed by Emilio 1997 and Domiciano de Souza Jr. 1999 and applied in Domiciano de Souza et al. 2000) and a Least-Squares (LS) fitting method.

The RLC method searches, in each wavelength bin, for 20 frequencies in a predefined range and computes all possible models with 4 frequencies. Comparing the power of each of these models, it selects 7 optimal frequencies while suppressing the aliases. A Local Cleanest (see Foster 1995) is then applied to these 7 values to finetune the final frequencies (see Neiner et al. 2002, for more details).

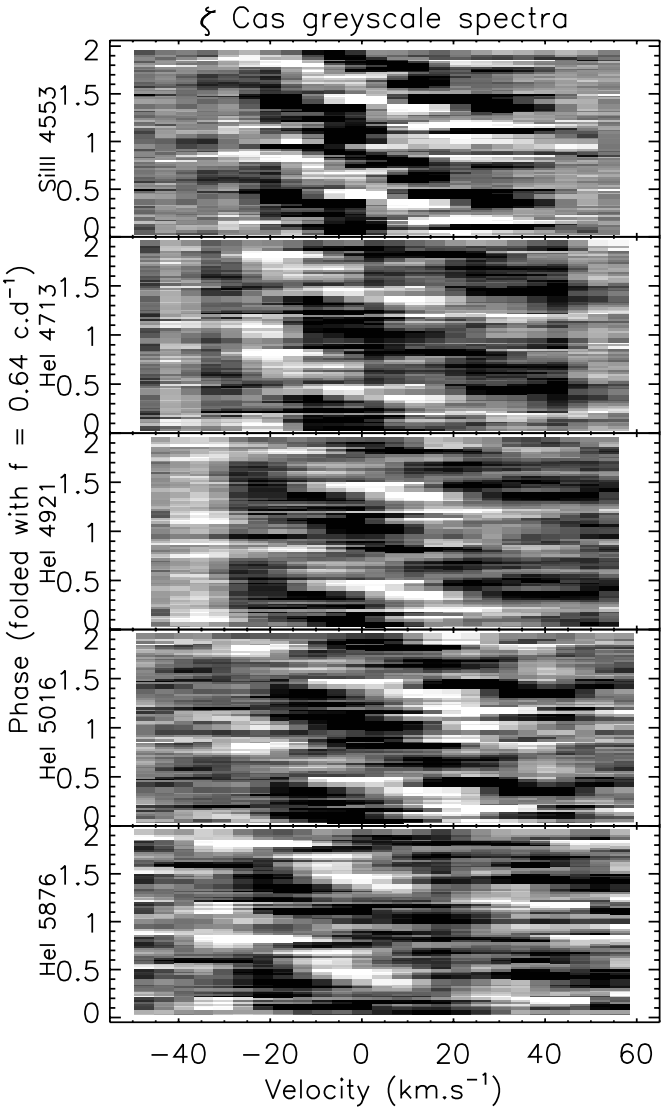

Fig. 4. Greyscale residual spectra, obtained by subtraction of the mean line-profile, folded in phase with the frequency $f = 0.64$ c d^{-1}.

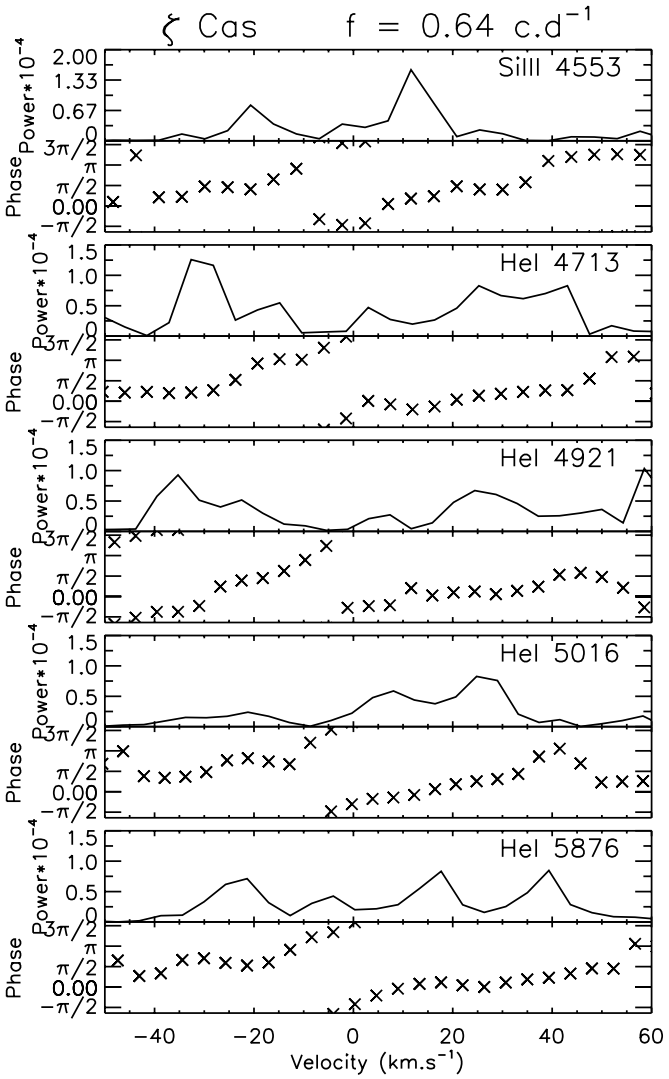

Fig. 5. Power and phase of the frequency $f = 0.64$ c d^{-1} over the profile of each studied line.

The LS method considers all wavelength bins over the full line width at the same time to determine which frequencies describe the variations in the best way. After a first frequency is found, the data are prewhitened, and the program looks for the next frequency in the residual spectra. This procedure is repeated several times.

Periods longer than the duration of the observing run ($P >$ 17 d, $f < 0.059$ c d^{-1}) cannot be detected. The mathematical frequency resolution of the frequency search method is better than 0.01 c d^{-1}, but the accuracy of the results due to the length of the run is 0.06 c d^{-1}.

In the data obtained in 2002, in all the studied lines, the frequency $f = 0.64$ c d^{-1} is found, together with its 1-day alias at $f = 1.64$ c d^{-1}. A greyscale plot of all the spectra for each studied line, from which the mean line-profile has been subtracted, is presented in Fig. 4, folded in phase with $f = 0.64$ c d^{-1}.

Figure 5 shows the power and phase of this frequency. From the slope of the phase through the line profile (see Neiner et al. 2002) we derive that these variations are associated with a non-radial pulsation mode with $l = 2 \pm 1$. $|m|$ cannot be derived because the power of the first harmonic is too weak. However, the positive phase slope combined with the fact that ζ Cas does not rotate very fast, suggests a retrograde mode.

Another weak frequency at $f = 1.21$ c d^{-1} is also detected which could be the first harmonic of $f = 0.64$ c d^{-1}.

Finally, plotting the residual spectra in phase with the rotation frequency $f_{\rm rot} = 0.186$ c d^{-1} reveals travelling features, which are associated with the two magnetic poles passing over the visible hemisphere of the star as it rotates (Fig. 6).

A frequency at 1.64 c d^{-1} is also detected in the data obtained in 2001, but these data are not well sampled in time, which makes the study of the pulsations more difficult.

5.2. Radial velocity

Figure 7 shows the variation in time of the radial velocity of the Si III 4553 and He I 4713, 4921, 5016 and 5876 lines. In general, all the He I lines and the Si III line vary in the same way, with a few exceptions especially for the He I 5876 line.

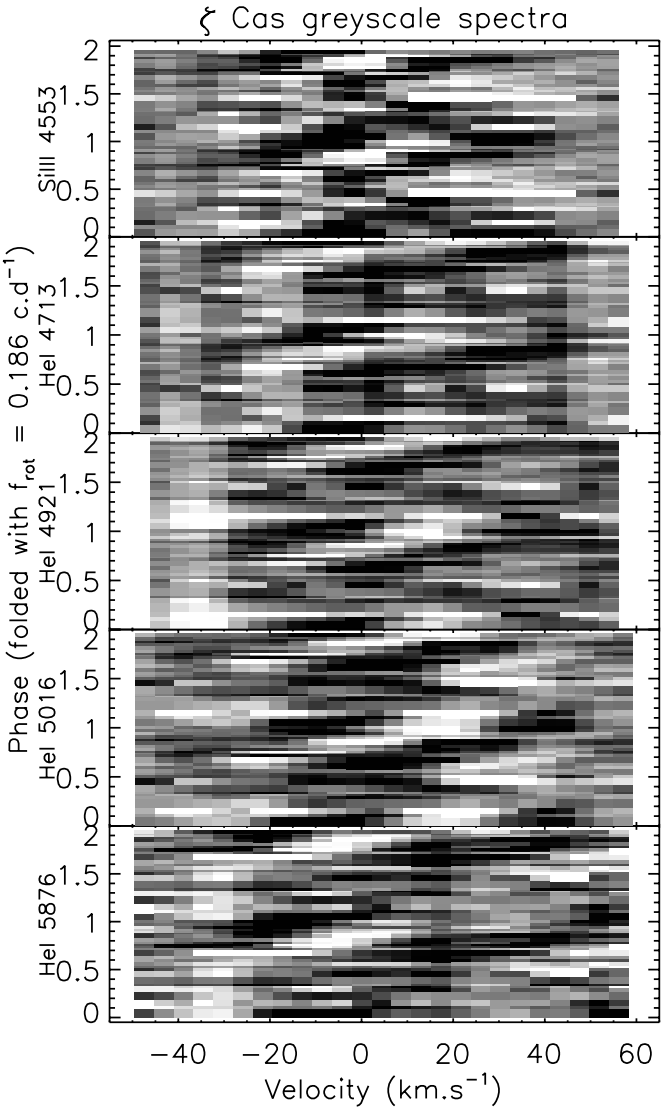

Fig. 6. Greyscale residual spectra, obtained by subtraction of the mean line-profile, folded in phase with the rotation frequency $f_{\rm rot}$ = 0.186 c d^{-1}. The travelling features are thought to be the result of the magnetic poles passing over the visible hemisphere of the star.

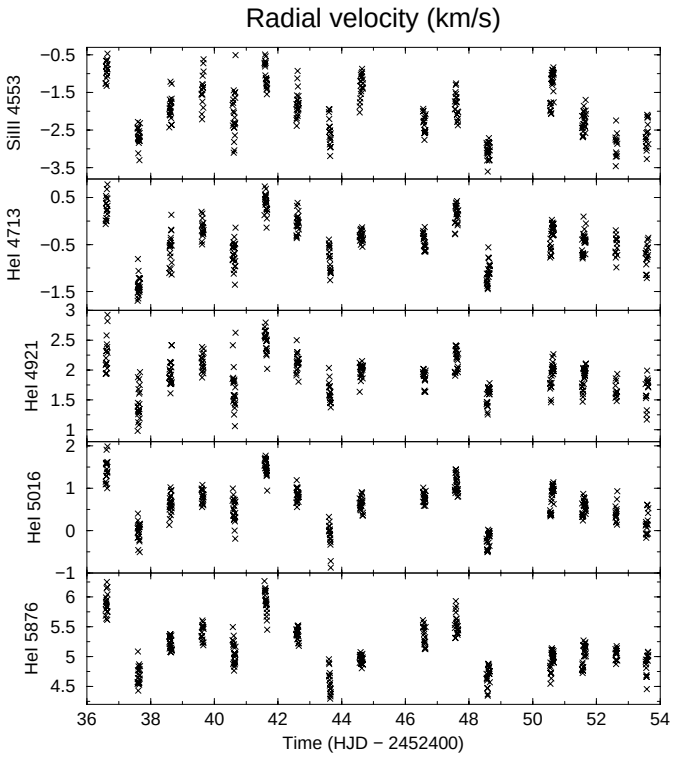

Fig. 7. Variation in time of the radial velocity of the Si III 4553 and He I 4713, 4921, 5016 and 5876 lines.

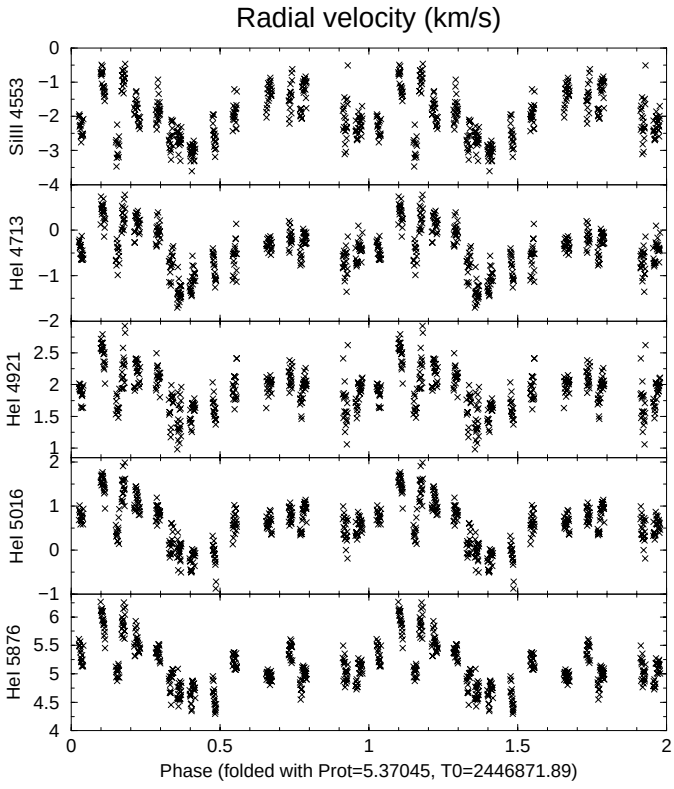

Fig. 8. Variation of the radial velocity of the Si III 4553 and He I 4713, 4921, 5016 and 5876 lines, folded in phase with $f_{\rm rot}$ using T_0 = 2 446 871.89.

Beating between the pulsation and rotation periods is expected at about 11 days but cannot be clearly identified within the 17-day run.

Figure 8 shows the same variation folded in phase with the rotational period. Although the signal is not fully periodic due to the pulsations, one could describe the behavior of the folded signal as having two minima around phases 0 and 0.5, and two maxima around phases 0.25 and 0.75. The amplitude of variations is very small, from 2 to 4 km s^{-1} depending on the line.

5.3. Minimum intensity

The minimum intensity (central depth) of the Si III 4553 and He I 4713, 4921, 5016 and 5876 lines shows variation in time.

Figure 9 shows these variations folded in phase with the rotational period. Similar to the radial velocity variations, all

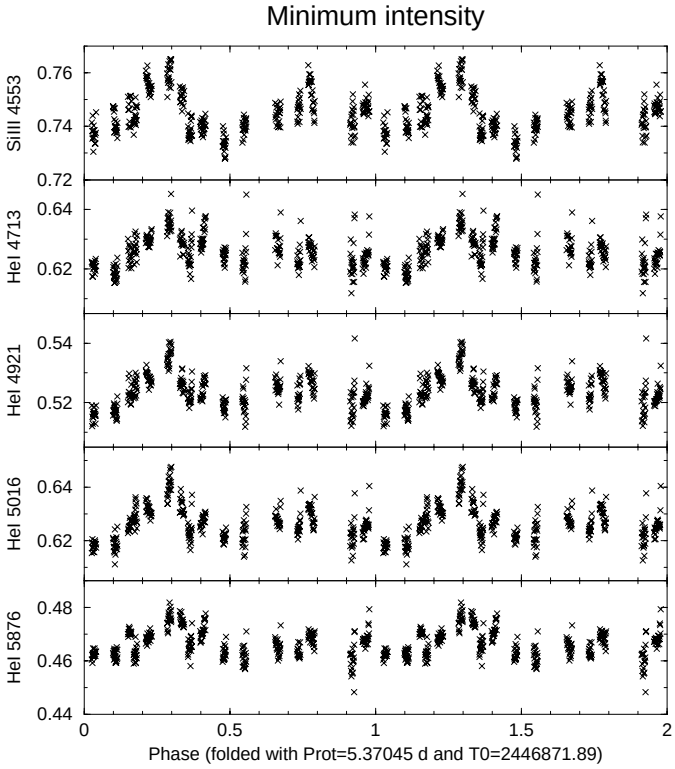

Fig. 9. Variation of the minimum intensity of the Si III 4553 and He I 4713, 4921, 5016 and 5876 lines, folded in phase with $f_{\rm rot}$ using $T_0 = 2\,446\,871.89$.

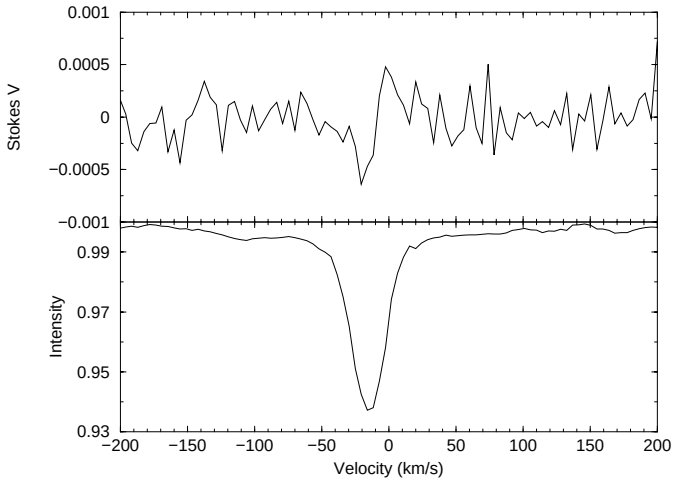

Fig. 10. Magnetic result for the measurement 71, which was taken close to the phase of minimum field. The top panel shows the Stokes V profile with the Zeeman signature. The bottom panel shows the mean photospheric line.

the He I lines and the Si III line vary roughly in the same way. Whether the apparent phase shift of 0.1 between the minima and maxima as compared to the extremes of the radial velocity measurements is significant, is not clear. The amplitude of variations is about 0.04 of the continuum intensity. Note that the He I 5876 line shows a smaller amplitude of variations, probably due to saturation.

6. Magnetic field

6.1. Detection

To avoid smearing of the magnetic signal due to pulsational effects, the individual exposure times had to be kept short. Nevertheless, thanks to the low $v \sin i$ and the relative brightness of the star, the error bars of the magnetic measurements are small and the Zeeman magnetic signature could be observed (Fig. 10).

Table 5 shows, for each measurement, the longitudinal magnetic field value B, its error bar σB, the null polarisation N and its error bar σN. The null polarisation N gives an indication of the pollution by non-stellar effects and should be zero for a perfect measurement. It is produced by associating the four subexposures of one magnetic measurement in the same way as for creating the Stokes V profile, except that the two last subexposures are exchanged.

The results are plotted in Fig. 11, folded in phase with the rotational period. A sine curve is overplotted, which shows the adopted best fit (with fixed period) to the data of 2001 and 2002 together, with a reduced $\chi^2 = 1.0$. The derived longitudinal field has an average value of $B_0 = -18 \pm 2$ G and amplitude $B_{\rm l} = 28 \pm 4$ G. We note that a fit with also the period as a free parameter yields the same values for the parameters and a value of 5.371 ± 0.004 d for the period, i.e. within the uncertainty equal to the adopted period from the UV data.

With the derived phase from the adopted fit we find for the ephemeris of maximum magnetic field strength:

$$T(B_{\rm max}) = \mathrm{HJD}\ 2\,452\,271.77 \pm 0.10 + N \times 5.370447 \pm 0.000078, \quad (3)$$

where N is an integer.

Comparison with the EW ephemeris (see Fig. 11) shows that the minimum (negative) magnetic field occurs 0.020 ± 0.029 in phase after the predicted epoch of minimum absorption of the UV wind lines. This expected minimum has an uncertainty of ± 0.025 in phase, i.e. in perfect agreement within the derived limits. Thus, the negative magnetic pole is oriented to the observer when the wind absorption is at minimum.

6.2. Oblique magnetic dipole

We have found a weak but significant varying longitudinal field in ζ Cas. This is consistent with an oblique magnetic dipole (see Shore 1987) with a rotational period of about 5.37 d.

For a dipolar field, the ratio of the magnetic extremes $r = B_{\rm max}/B_{\rm min}$ is related to the inclination angle i and the angle between the magnetic and the rotation axis β via (Shore 1987)

$$r = \frac{\cos(i+\beta)}{\cos(i-\beta)}. \quad (4)$$

In the case of ζ Cas we find $r = -0.20 \pm 0.14$. If we adopt the inclination angle $i = 18 \pm 4^\circ$ derived in Sect. 4, we obtain $\beta = 77 \pm 6^\circ$.

Table 5. Longitudinal magnetic field measurements.

#	Phase	B	σB	N	σN	#	Phase	B	σB	N	σN	#	Phase	B	σB	N	σN	#	Phase	B	σB	N	σN
1	0.254	10	21	−11	19	31	0.688	21	26	16	24	61	0.742	3	35	6	33	91	0.218	−33	19	4	18
2	0.257	−10	20	−2	19	32	0.048	−83	27	6	25	62	0.916	−83	54	65	54	92	0.222	−25	20	13	18
3	0.817	6	26	7	25	33	0.051	−36	28	44	27	63	0.919	−7	53	−84	52	93	0.227	−18	20	−2	19
4	0.820	−50	26	32	25	34	0.428	27	24	−15	23	64	0.922	−10	53	6	52	94	0.231	−25	19	−6	19
5	0.823	−24	29	38	27	35	0.431	7	25	7	23	65	0.925	−4	54	−28	53	95	0.400	10	20	32	18
6	0.999	−69	54	−18	54	36	0.808	−42	24	−21	22	66	0.929	−2	59	−55	59	96	0.404	−0	21	−13	20
7	0.002	−25	29	23	27	37	0.811	−12	24	26	23	67	0.102	−61	35	24	33	97	0.408	5	22	3	21
8	0.006	−10	24	5	23	38	0.546	34	23	20	22	68	0.105	−57	29	−30	27	98	0.412	25	25	−3	23
9	0.009	−12	24	−4	23	39	0.549	14	23	−18	22	69	0.108	−37	27	−3	26	99	0.416	22	28	8	27
10	0.193	14	63	2	62	40	0.085	−38	32	4	31	70	0.111	−54	27	−9	25	100	0.771	−28	20	4	19
11	0.380	−41	34	−22	34	41	0.266	−13	22	−8	21	71	0.114	−91	29	5	27	101	0.775	−9	20	−22	19
12	0.383	15	41	−80	40	42	0.269	14	22	15	20	72	0.287	7	29	−7	28	102	0.779	−46	22	−4	21
13	0.564	2	24	−29	22	43	0.454	7	25	25	24	73	0.290	6	30	11	28	103	0.783	−27	21	2	20
14	0.567	41	28	39	26	44	0.457	15	26	−46	25	74	0.293	−86	30	−24	29	104	0.787	−62	23	−27	21
15	0.570	−16	31	−8	30	45	0.172	−33	26	−1	25	75	0.296	−46	31	−26	29	105	0.790	−8	26	37	25
16	0.749	13	27	−4	25	46	0.175	−13	34	21	33	76	0.299	6	32	48	31	106	0.958	−58	21	−20	21
17	0.752	−6	28	−20	27	47	0.178	−89	44	60	45	77	0.477	20	26	7	25	107	0.962	−47	19	−23	18
18	0.756	−3	23	−7	21	48	0.181	5	30	8	29	78	0.480	−11	26	−12	24	108	0.966	−62	20	−26	19
19	0.935	11	27	28	25	49	0.358	−12	30	10	29	79	0.483	15	26	−10	24	109	0.970	−72	20	−13	19
20	0.938	−2	29	−45	28	50	0.361	−59	30	25	29	80	0.486	17	25	−12	24	110	0.974	−44	20	3	19
21	0.942	−33	30	−4	29	51	0.364	−24	32	−56	31	81	0.657	−12	24	−2	23	111	0.978	−57	24	−10	23
22	0.122	−57	32	17	31	52	0.367	33	35	−36	34	82	0.662	−57	24	−19	23	112	0.153	3	32	4	31
23	0.126	10	27	−0	26	53	0.370	−9	34	−18	33	83	0.666	1	26	−21	25	113	0.157	6	34	−16	34
24	0.129	−64	33	19	32	54	0.544	−1	43	−11	42	84	0.670	−58	25	−16	24	114	0.161	−54	33	17	32
25	0.308	49	30	−42	28	55	0.547	1	40	8	39	85	0.673	−57	29	−2	28	115	0.330	29	27	−0	26
26	0.312	55	26	−17	25	56	0.553	33	39	−51	38	86	0.028	−72	28	−32	27	116	0.334	−41	25	−15	24
27	0.315	7	32	−39	31	57	0.556	19	44	61	44	87	0.032	−30	25	−22	24	117	0.339	−42	25	−1	24
28	0.313	22	45	−50	44	58	0.733	−76	35	54	33	88	0.036	−87	27	68	26	118	0.343	−20	30	−2	30
29	0.316	−38	41	20	40	59	0.736	−31	33	46	32	89	0.040	−82	27	12	26						
30	0.685	−27	25	−33	23	60	0.739	−22	28	−2	26	90	0.214	7	19	1	17						

The observed phase difference $\Delta\Phi$ between the two UV maxima is also related to the angles i and β via (Shore 1987)

$$\cos\frac{\Delta\Phi}{2} = \frac{1}{\tan i \tan\beta}. \quad (5)$$

In the case of ζ Cas we find $\Delta\Phi = 0.323 \pm 0.037$ from the analytical fit (Eq. (1)) shown in Fig. 11. If we adopt the inclination angle $i = 18 \pm 4°$ derived in Sect. 4, we obtain $\beta = 80 \pm 4°$.

These two determinations of the angle β are in good agreement. In the following, we will assume the mean value $\beta = 79 \pm 3°$.

When two maxima are observed in the UV equivalent width variations, it is expected that $i + \beta > 90°$. If there is only one maximum, then only one magnetic pole crosses the line of sight over the visible hemisphere, and $i + \beta < 90°$. For ζ Cas, we can clearly distinguish two maxima, although the secondary minimum is not deep. Therefore we expect that the second pole appears only at the edge of the visible hemisphere and that $i + \beta$ does not exceed 90° by a large amount. Indeed, we find that $i + \beta = 97 \pm 7°$.

6.3. Model

Knowledge of the angles i and β in an oblique magnetic dipole model allows us to derive the strength of the polar magnetic field which would reproduce the values of longitudinal field measured at TBL. The model we use is described in Neiner et al. (2003).

Using a limb darkening factor $k = 0.4$ as established by Claret (2000) for this kind of stars in the optical, $i = 18 \pm 4°$ as derived in Sect. 4 and $\beta = 79 \pm 3°$ obtained above, we model a centered oblique rotator model and fit it to the longitudinal magnetic field data. The best fit is obtained with $B_0 = -18 \pm 2$ G, $B_l = 30 \pm 3$ G and a polar field $B_{pol} = 335^{+120}_{-65}$ G, with a reduced $\chi^2 = 1.0$. The values obtained for B_0 and B_l are compatible with the ones obtained from the best sine fit in Sect. 6.1, with a similar χ^2 value. Note that the angles i and β

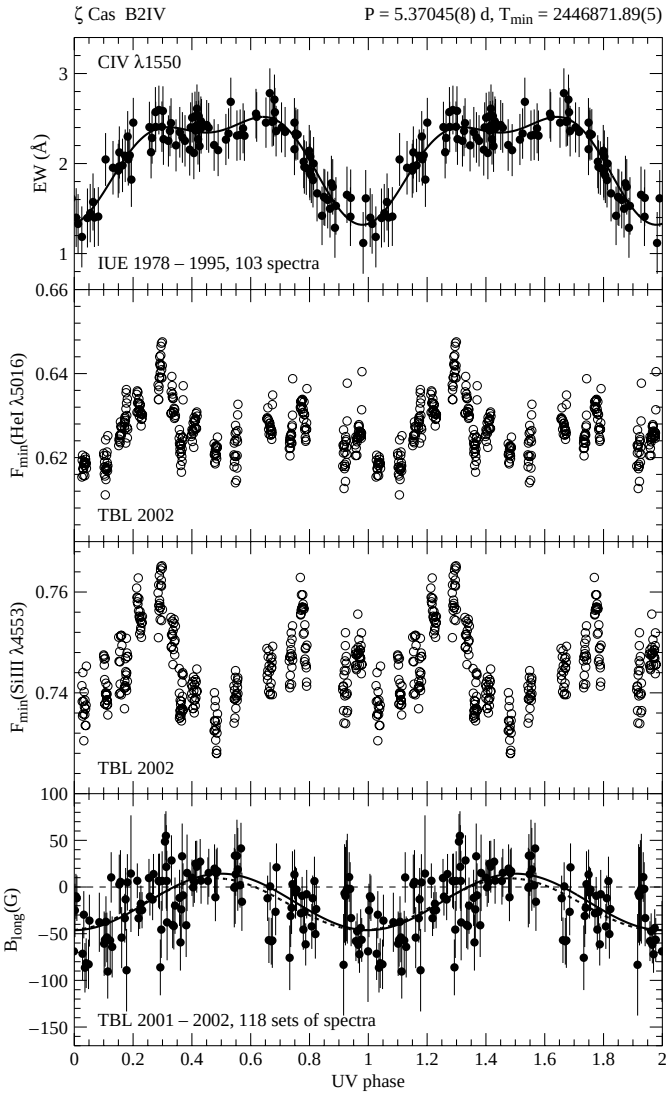

Fig. 11. Top panel: variation of the equivalent width of the UV C IV line. The best fit of a double sine wave (Eq. (1)) is overplotted. Middle panels: variation of the minimum intensity of the He I 5016 and Si III 4553 lines. Bottom panel: variation of the longitudinal component of the magnetic field, averaged over the stellar disk. The best sine fit (dashed line) and the dipole model (solid line) are overplotted. All plots are folded in phase with the rotation period.

are anticorrelated, i.e. to keep B_0 and B_l constant with decreasing i, β and $B_{\rm pol}$ have to be increased.

A greyscale plot of the longitudinal component of the magnetic field on the visible hemisphere of the star, at different rotational phases, is shown in Fig. 12.

7. Conclusions and discussion

7.1. Pulsations

We investigated the periodic variations of ζ Cas in the line-profile variations, radial velocity and minimum intensity measurements of the He I 4713, 4921, 5016 and 5876 and Si III 4553 lines. From the data obtained in 2002, we found that the star pulsates non-radially with a period of 1.56 d (f = 0.64 c d^{-1}). This period seems to be also present in the data obtained in 2001. We associate it with a non-radial pulsation mode with $l = 2 \pm 1$, probably retrograde.

The periods previously published in the literature were not found in our dataset. Non-stable periods of the order of 1 day associated with non-radial pulsations are typical for SPB stars and we therefore propose to classify ζ Cas as a SPB star.

Pamyatnykh (1999) calculated the border of the SPB instability strip in the HR diagram using new opacity determinations. From his Fig. 4 and the parameters of the star, we see that ζ Cas lies in the region of the HR diagram that belongs both to the SPB instability strip and the β Cep instability strip.

7.2. Rotation

From the analysis of the behavior of the stellar wind lines of C IV in 103 IUE spectra we determined a precise value of the rotation period $P_{\rm rot}$ = 5.37045 d.

This period was also found in the lpv. Folding the measurements of radial velocity and minimum intensities with this period reveals 2 maxima and 2 minima (Figs. 8 and 9). Such variations in phase with the rotation period have also been observed in the β Cep star V2052 Oph (Neiner et al. 2003). For V2052 Oph this behavior was interpreted in the frame of an oblique magnetic rotator with a magnetically confined wind, considering the geometrical position of the magnetic poles and magnetic equator on the visible hemisphere of the star as it rotates (Neiner et al. 2003). The same model would apply for ζ Cas.

7.3. Magnetic field

We searched for a magnetic field in ζ Cas and obtained clear Zeeman signatures indicative of the presence of a magnetic field in this star (Fig. 10).

The observed longitudinal component of the magnetic field varies sinusoidally with the rotation period, in accordance with the magnetic oblique dipole model. The best-fit values are -18 ± 2 G for the mean longitudinal field and 28 ± 4 G for the amplitude (Fig. 11). A comparison of the phase of UV minimum in *EW* and of the phase of maximum field shows a very good agreement.

From a single measurement Landstreet (1982) obtained a non detection of the magnetic field of ζ Cas of $B = 70 \pm 310$ G at HJD = 2 441 560.83. This corresponds to phase 0.06 in our magnetic curve. At this phase, the expected field is about $B = -48 \pm 3$ G, consistent with Landstreets value. This illustrates that one cannot conclude the absence of a magnetic field from a single non-detection.

We found that the axis of the dipole is inclined with the angle $\beta = 79 \pm 3°$ compared to the rotation axis with inclination $i = 18 \pm 4°$. The amplitude of variations of the mean longitudinal component of the magnetic field averaged over the stellar disk is weak due to this specific geometrical orientation with respect to the observer's line-of-sight.

With our dipole code we derived that the strength of the polar magnetic field is $B_{\rm pol} = 335^{+120}_{-65}$ G. This is close to the theoretical value of 300 G obtained by Cassinelli et al. (2002)

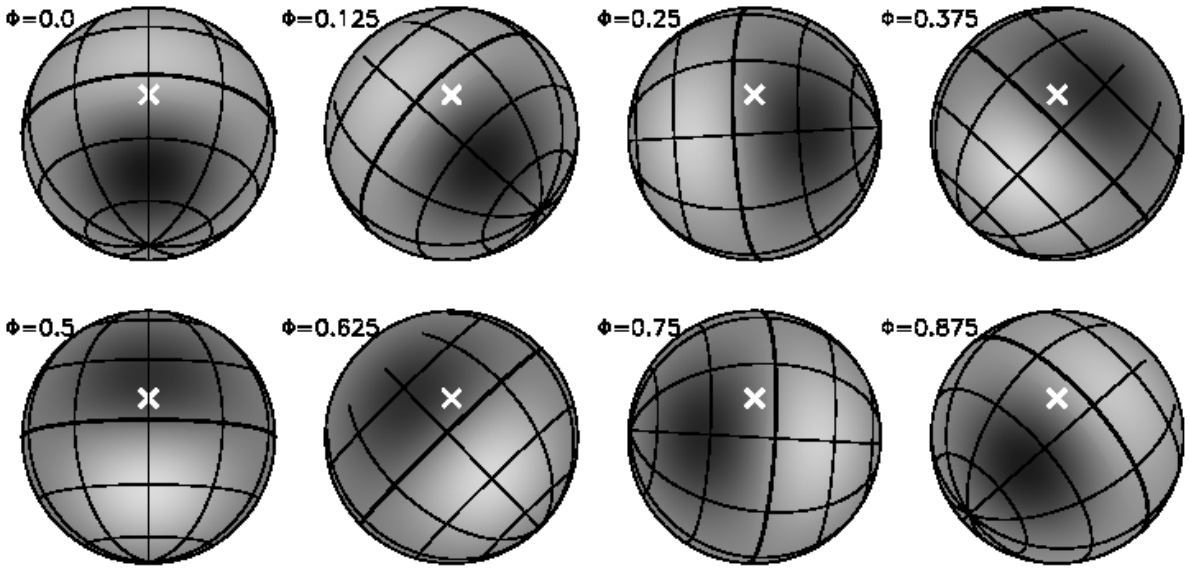

Fig. 12. Greyscale representation of the relative contribution of the magnetic dipole to the integrated longitudinal magnetic field on the visible hemisphere of ζ Cas, at different rotational phases with steps of $\delta\Phi = 0.125$. The black color corresponds to positive field values and the white color to negative field values. The phase runs from the top left panel to the lower right panel and corresponds to the convention used in Fig. 11. A grid of magnetic longitudes and latitudes is overplotted, with the magnetic equator shown as a thicker black line. The rotation axis is shown with a white cross. Although the magnetic field is strongest at the magnetic poles, the positions on the stellar surface that contribute the most to the longitudinal field are not at the poles, due to a geometrical effect and to the limb darkening effect.

for a B2 V star to form a magnetically torqued disk in rapidly rotating stars.

However, we find that the rotational velocity of ζ Cas is 55 ± 28 km s^{-1}, i.e. the star does not rotate close to its breakup velocity. In addition, no evidence for a disk around this star is known from IR or X-ray data. The IR flux of ζ Cas measured by IRAS is 0.7 Jy at 12 μm. Corrected for the slope of the stellar spectrum, this corresponds to 0.5 Jy. The predicted 12 μm flux based on a Rayleigh-Jeans extrapolation of photometric data (Glushneva et al. 1992) up to 1 μm is 0.5 Jy (S. Hony, priv. comm.). Therefore there is no IR excess detected in this star. Berghoefer et al. (1996) give an upper limit of the X-ray emission from ROSAT observations of $\log L_X/L_{\rm bol} = -7.92$. The value obtained for β Cep, a similar star which has a disk, is $\log L_X/L_{\rm bol} = -7.16$. This means that if ζ Cas would have a similiar X-ray flux as β Cep, ROSAT would have detected the source. We conclude that ζ Cas does not show evidence for the presence of a disk.

7.4. Chemical abundances

We confirm that ζ Cas is N-enriched. We also find that it is slightly overabundant in He.

A comparison of ζ Cas with the two known magnetic early-B stars β Cep and V2052 Oph is interesting. All three stars show departures from solar abundances. In particular both β Cep and ζ Cas are N-enriched. Peculiar chemical abundances are usually found in magnetic stars, in which microscopic diffusion effects allow elements with a high atomic mass to sink in the atmosphere under the dominant influence of gravity, while elements which can absorb photons of many wavelengths from the outward flow of radiation through the star are lifted towards the surface. The presence of a magnetic field inhibits mixing motions in the outer layers, and hence produces chemical peculiarities.

Cayrel de Strobel et al. (1997) reported that ζ Cas has a low metal abundance of [Fe/H] = 0.48. Fitzpatrick & Massa (1999) found similar results with [Fe/H] = 0.15. A low metal abundance was also found in V2052 Oph (Smith & Groote 2001). Moreover Proffitt et al. (1999) found that the abundance of B is extremely low ($\log \epsilon(B) = -1.43$ relative to the Sun) in ζ Cas. This provides accumulating evidence that magnetic fields play a major role in the chemical stratification of these stars.

The results presented in this paper make ζ Cas the third discovered magnetic pulsating B star and first known magnetic SPB star. Such stars are apparently rather rare, but will provide the most massive examples of stars useful for asteroseismological (and hence evolutionary) tests.

Future work should include better time resolved optical spectra to study the pulsation properties of the star and to investigate the stability of the period.

Acknowledgements. We wish to thank J.-F. Donati and his colleagues for providing additional TBL data. YF is supported by a Marie Curie Individual Fellowship of the European Community programme FP5 under contract number HPMF-CT-2000-00497. This research has made use of the Simbad database maintained at CDS, Strasbourg, France.

References

Andrievsky, S. M., Korotin, S. A., Luck, R. E., & Kostynchuk, L. Y. 1999, A&A, 350, 598

Berghoefer, T. W., Schmitt, J. H. M. M., & Cassinelli, J. P. 1996, A&AS, 118, 481

Cardelli, J. A., Clayton, G. C., & Mathis, J. S. 1989, ApJ, 345, 245

Cassinelli, J. P., Brown, J. C., Maheswaran, M., Miller, N. A., & Telfer, D. C. 2002, ApJ, 578, 951

Cayrel de Strobel, G., Soubiran, C., Friel, E. D., Ralite, N., & Francois, P. 1997, A&AS, 124, 299

Chalabaev, A., & Maillard, J. P. 1983, A&A, 127, 279

Claret, A. 2000, A&A, 363, 1081

Dimitrijevic, M. S., Djenize, S., Sreckovic, A., & Bukvic, S. 2003, in IAU Symp. 210, Modelling of Stellar Atmospheres, held in Sweden in 2002, in press

Domiciano de Souza, A., Janot-Pacheco, E., Leister, N. V., et al. 2000, in The Be Phenomenon in Early-Type Stars, IAU Colloq. 175, ed. M. A. Smith, H. F. Henrichs, & J. Fabregat, ASP Conf. Ser., 214, 276

Domiciano de Souza Jr., A. 1999, Master's Thesis, IAG-USP, Brazil

Donati, J.-F., Catala, C., Wade, G. A., et al. 1999, A&AS, 134, 149

Donati, J.-F., Semel, M., Carter, B. D., Rees, D. E., & Collier Cameron, A. 1997, MNRAS, 291, 658

Duflot, M., Figon, P., & Meyssonnier, N. 1995, A&AS, 114, 269

Emilio, M. 1997, Master's Thesis, IAG-USP, Brazil

Fitzpatrick, E. L., & Massa, D. 1999, ApJ, 525, 1011

Foster, G. 1995, AJ, 109, 1889

Foster, G. 1996, AJ, 111, 541

Garcia, B. 1989, Bulletin d'Information du Centre de Données Stellaires, 36, 27

Gies, D. R., & Lambert, D. L. 1992, ApJ, 387, 673

Glushneva, I. N., Kharitonov, A. V., Kniazeva, L. N., & Shenavrin, V. I. 1992, A&AS, 92, 1

González, V. R., Aparicio, J. A., & del Val, J. A. 2000, A&A, 363, 1177

Grady, C. A., Bjorkman, K. S., & Snow, T. P. 1987, ApJ, 320, 376

Grevesse, N., & Sauval, A. J. 1998, Space Sci. Rev., 85, 161

Henrichs, H. F. 2001, in Magnetic Fields Across the Hertzsprung-Russell Diagram, held in Santiago in 2001, ed. G. Mathys, S. K. Solanki, & D. T. Wickramasinghe, ASP Conf. Ser., 248, 393

Henrichs, H. F., de Jong, J. A., Donati, J.-F., et al. 2000, in The Be Phenomenon in Early-Type Stars, IAU Coll. 175, ed. M. A. Smith, H. F. Henrichs, & J. Fabregat, ASP Conf. Ser., 214, 324

Henrichs, H. F., Kaper, L., & Nichols, J. S. 1994, A&A, 285, 565

Hoffleit, D., & Jaschek, C. 1991, The Bright star catalogue (New Haven, Conn.: Yale University Observatory), 5th rev. ed., ed. D. Hoffleit, & C. Jaschek

Hubeny, I., & Lanz, T. 1995, ApJ, 439, 875

Korotin, S. A., Andrievsky, S. M., & Luck, R. E. 1999, A&A, 351, 168

Kurucz, R. 1994, CD-ROM No. 19. (Cambridge, Mass.: Smithsonian Astrophysical Observatory)

Landstreet, J. D. 1982, ApJ, 258, 639

Lanz, T., Dimitrijevic, M. S., & Artru, M.-C. 1988, A&A, 192, 249

Merezhin, V. P. 2000, Ap&SS, 274, 581

Neiner, C., Henrichs, H. F., Floquet, M., et al. 2003, A&A, in press

Neiner, C., Hubert, A.-M., Floquet, M., et al. 2002, A&A, 388, 899

O'Donnell, J. E. 1994, ApJ, 422, 158

Pamyatnykh, A. A. 1999, Acta Astron., 49, 119

Papaj, J., Wegner, W., & Krelowski, J. 1990, MNRAS, 246, 408

Perryman, M. A. C., & ESA. 1997, The HIPPARCOS and TYCHO catalogues (Noordwijk, The Netherlands: ESA Publications Division), Series: ESA SP Ser. 1200

Proffitt, C. R., Jönsson, P., Litzén, U., Pickering, J. C., & Wahlgren, G. M. 1999, ApJ, 516, 342

Rountree, J., & Sonneborn, G. 1991, ApJ, 369, 515

Sadsaoud, H., Le Contel, J. M., Chapellier, E., Le Contel, D., & Gonzalez-Bedolla, S. 1994, A&A, 287, 509

Schaller, G., Schaerer, D., Meynet, G., & Maeder, A. 1992, A&AS, 96, 269

Shore, S. N. 1987, AJ, 94, 731

Smith, M. A. 1980, in Nonradial and Nonlinear Stellar Pulsation, Workshop held in Tucson in 1979, 60

Smith, M. A., & Groote, D. 2001, A&A, 372, 208

Smith, M. A., & Karp, A. H. 1976, Solar and Stellar Pulsation, 6544, 289

Sonneborn, G., Garhart, M. P., & Grady, C. A. 1987, in Physics of Be Stars, held in Boulder in 1986, ed. A. Slettebak, & T. P. Snow, IAU Colloq., 92, 286 (Cambridge University Press)

Waelkens, C. 1991, A&A, 246, 453